Comparison of Anisotropic Energy-based and Jiles-Atherton Models of Ferromagnetic Hysteresis

B. Upadhaya[1], P. Rasilo[2], L. Perkkiö[3], P. Handgruber[4], A. Belahcen[1], and A. Arkkio[1]
[1]Department of Electrical Engineering and Automation, Aalto University, P. O. Box 15500, FI-00076 Aalto, Finland
[2]Unit of Electrical Engineering, Tampere University, P. O. Box 692, FI-33014 Tampere University, Tampere, Finland
[3]Department of Mathematics and Systems Analysis, Aalto University, P. O. Box 11100, FI-00076 Aalto, Finland
[4]Institute of Fundamentals and Theory in Electrical Engineering, Graz University of Technology, Graz, A-8010, Austria

In this paper, we apply an anisotropic extension for the energy-based and the Jiles-Atherton hysteresis models to simulate both unidirectional alternating and rotational magnetic field excitations. The results show a good agreement with measurements for unidirectional alternating fields. However, the results for rotational fields, especially at high magnitudes, show a significant discrepancy with the measurement data. We demonstrate that the Jiles-Atherton model with appropriate parameters can estimate the losses in alternating cases up to 1.5 T, whereas both models give reasonable loss estimation up to 1 T in rotational cases.

Index Terms—**Energy-based Model, Jiles-Atherton Model, Magnetic Hysteresis, Non-oriented Electrical Steel.**

I. Introduction

ACCURATE modeling of hysteresis phenomena is important for efficient design of electromagnetic devices, and different types of ferromagnetic hysteresis models have been developed for different applications. Among existing models, the energy-based (EB) model is particularly attractive [1]–[4], as it combines advantages of both Preisach and Jiles-Atherton (JA) models [3], [5]–[7]. The EB model is derived from thermodynamic principles, and at any moment, the stored and dissipated magnetic energy is known (as opposed to the JA model). In addition, the model is readily vectorial. Another advantage is that the memory effect is present, which yields a better representation of non-symmetric minor loops. The model considers the magnetic field strength H as the input variable. Unlike the Preisach and JA models, the EB model is not easily invertible to use magnetic flux density input [8]–[11]. Therefore, the model must be inverted numerically for a numerical field analysis that utilizes the magnetic flux density B as the primary variable [8].

In this paper, the anisotropic EB and JA hysteresis models are briefly discussed. The anisotropic extension is realized using parameters and anhysteretic characteristics in the rolling and transverse directions of the silicon steel sheet. The parameters of the EB model are identified from the unidirectional alternating magnetic measurements. The identification procedure utilizes the auxiliary function approach presented in [12]. The JA model parameters are estimated from all the measured symmetric minor and major BH loops corresponding to the unidirectional alternating field. The parameters are computed using a combination of heuristic optimization techniques [13]–[15].

Since the EB model defines hysteresis loss dissipation as a direct consequence of the domain wall pinning, an idea intrinsic to the JA model, a comparison with the JA model is insightful. In this paper, the accuracy in the simulation of the symmetric minor BH loops and the corresponding hysteresis losses is investigated. Also, the measured rotational magnetic characteristics and the corresponding losses are compared with simulation results. The BH measurement data used in this paper corresponds to 0.5 mm non-oriented (NO) silicon-iron electrical steel (grade M400-50A). The magnetic measurements are obtained from a rotational single-sheet tester (RSST) [16], [17]. The measurement is a B-controlled and performed at 50 Hz. An approximation of the quasi-static magnetic field is obtained by removing the classical eddy-current loss field from the measured field strength [18]. It should be noted that the models in this paper are limited to the rate-independent case.

Manuscript received August 27, 2019; revised November 19, 2019 and December 31, 2019; accepted January 4, 2020. Date of publication January XX, 2020; date of current version January XX, 2020. Corresponding author: Brijesh Upadhaya (email: brijesh.upadhaya@aalto.fi).

II. Energy-based Hysteresis Model

A detailed derivation of the EB model can be found in [3], [4], [19]–[21]. The magnetic flux density in a material is expressed as

$$\boldsymbol{B} = \mu_0 \boldsymbol{H} + \mu_0 \boldsymbol{M} = \mu_0 \boldsymbol{H} + \boldsymbol{J}, \tag{1}$$

where μ_0 is the permeability of free space, $\boldsymbol{J}$ is the material magnetic polarization, $\boldsymbol{M}$ is the material magnetization, and $\boldsymbol{H}$ is the magnetic field strength. The magnetic material is considered to be a collection of sub-systems (or pseudo-particles), and the resultant magnetic polarization is a sum of contributions from all the sub-systems,

$$\boldsymbol{J} = \sum_{\ell=1}^{N} \boldsymbol{J}^{\ell} = \sum_{\ell=1}^{N} \left(\omega_{\mathrm{x}}^{\ell} J_{\mathrm{an,x}}^{\ell} \mathbf{e}_{\mathrm{x}} + \omega_{\mathrm{y}}^{\ell} J_{\mathrm{an,y}}^{\ell} \mathbf{e}_{\mathrm{y}} \right), \tag{2}$$

where

$$\mathbf{e}_{\mathrm{x}} = (H_{\mathrm{rev,x}} / \|\boldsymbol{H}_{\mathrm{rev}}\|)\hat{e}_{\mathrm{x}}, \text{ and } \mathbf{e}_{\mathrm{y}} = (H_{\mathrm{rev,y}} / \|\boldsymbol{H}_{\mathrm{rev}}\|)\hat{e}_{\mathrm{y}}.$$

The pinning field probability densities $\omega_{\mathrm{x}}^{\ell}$, $\omega_{\mathrm{y}}^{\ell} > 0$ are associated with the pinning field strengths $\kappa_{\mathrm{x}}^{\ell}$, $\kappa_{\mathrm{y}}^{\ell}$ and satisfy

$$\sum_{\ell=1}^{N} \omega_{\mathrm{x}}^{\ell} = 1, \quad \text{and} \quad \sum_{\ell=1}^{N} \omega_{\mathrm{y}}^{\ell} = 1.$$

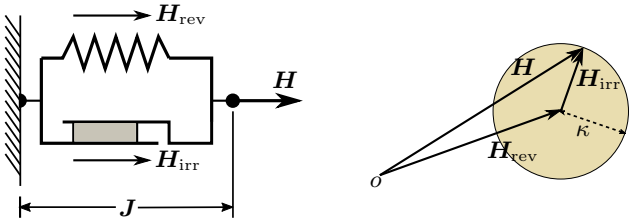

Fig. 1. Schematic of energy-based hysteresis model. A mechanical analogy with a spring-slider system (left), and a single particle model (right).

The anhysteretic polarizations

$$J^{\ell}_{\rm an,x} = f_{\rm x}(\|\boldsymbol{H}_{\rm rev}\|) \quad \text{and} \quad J^{\ell}_{\rm an,y} = f_{\rm y}(\|\boldsymbol{H}_{\rm rev}\|)$$

represent the anhysteretic characteristic of the magnetic material in the rolling and transverse directions.

The update rule of the reversible magnetic field strength (the memory vector) is

$$\boldsymbol{H}^{\ell}_{{\rm rev},t+\Delta t} = \begin{cases} \boldsymbol{H}^{\ell}_{{\rm rev},t}, \text{ if } \| \left[\boldsymbol{\kappa}^{\ell}\right]^{-1} \partial \boldsymbol{H}^{\ell} \| \leq 1, \\ \boldsymbol{H} - \boldsymbol{\kappa}^{\ell} \mathbf{e}_{\boldsymbol{H}^{\ell}_{\rm irr}}, \text{ otherwise,} \end{cases} \tag{3}$$

where $\partial \boldsymbol{H}^{\ell} = \boldsymbol{H} - \boldsymbol{H}^{\ell}_{{\rm rev},t}$, $\mathbf{e}_{\boldsymbol{H}^{\ell}_{\rm irr}} = \frac{\boldsymbol{J}^{\ell}}{\|\boldsymbol{J}^{\ell}\|}$, $\boldsymbol{\kappa}^{\ell} = \begin{bmatrix} \kappa^{\ell}_{\rm x} & 0 \\ 0 & \kappa^{\ell}_{\rm y} \end{bmatrix}$, $\boldsymbol{H}^{\ell}_{\rm irr}$ is the irreversible magnetic field strength. The correct direction $\mathbf{e}_{\boldsymbol{H}^{\ell}_{\rm irr}} = \cos(\alpha)\hat{\boldsymbol{e}}_{\rm x} + \sin(\alpha)\hat{\boldsymbol{e}}_{\rm y}$ is searched utilizing (2) and the explicit update rule [21], [22]

$$\boldsymbol{H}^{\ell}_{{\rm rev},t+\Delta t} = \begin{cases} \boldsymbol{H}^{\ell}_{{\rm rev},t}, \text{ if } \| \left[\boldsymbol{\kappa}^{\ell}\right]^{-1} \partial \boldsymbol{H}^{\ell} \| \leq 1, \\ \boldsymbol{H} - \boldsymbol{\kappa}^{\ell} \dfrac{\boldsymbol{\kappa}^{\ell} \partial \boldsymbol{H}^{\ell}}{\|\boldsymbol{\kappa}^{\ell} \partial \boldsymbol{H}^{\ell}\|}, \text{ otherwise.} \end{cases} \tag{4}$$

The EB model with explicit update rule (4) is a so-called vector play type model (VPM) [23], [24]. In this paper, (4) is used to simulate the unidirectional alternating magnetic excitations, whereas (3) is used to simulate rotational magnetic field excitations. For brevity, in this paper, the EB model having (3) as an update rule is called EBM (in the literature, some authors prefer to call it a full differential approach [21]).

Fig. 1 is a mechanical analogy of the single-particle EB model. It consists of a spring connected to a friction slider (or damper). In a multi-particle (or cells/sub-systems) EB model, the spring-damper units are connected in series. Thus, for a N particle system, there are $N-1$ spring-damper units, and the remaining one is spring without any damper. The single-particle model is a representation of isotropic media. Therefore, for an anisotropic medium the shape of the particle region could be ellipsoidal and various other shapes (see, e.g., [25, Fig. 3 and 4] for a detailed overview).

III. Jiles-Atherton Hysteresis Model

The vector modification of the original scalar JA model is presented in [11], [26]. The following equations describe the vector JA hysteresis model:

$$\boldsymbol{B} = \mu_0(\boldsymbol{H} + \boldsymbol{M}), \tag{5}$$

$$\frac{\partial \boldsymbol{B}}{\partial \boldsymbol{H}} = \mu_0 \mathbf{I} + \mu_0 \frac{\partial \boldsymbol{M}}{\partial \boldsymbol{H}}, \tag{6}$$

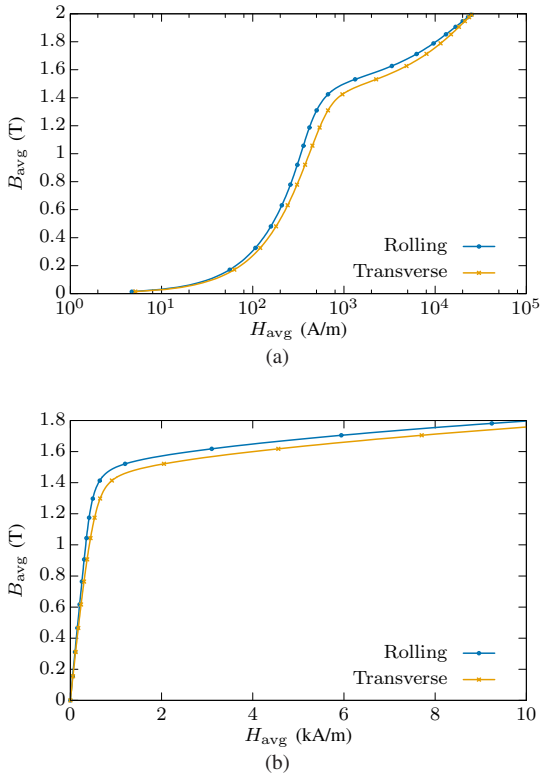

Fig. 2. Anhysteretic magnetization in the rolling and transverse directions of the NO silicon steel sheet. The anhysteretic curves are extracted from the measured major BH loops. (a) Logarithmic plot. (b) Linear plot for $H_{\rm avg} \leq 10$ kA/m.

$$\frac{\partial \boldsymbol{M}}{\partial \boldsymbol{H}} = \left[\mathbf{I} - (\boldsymbol{\chi} + \boldsymbol{c\xi})\,\boldsymbol{\alpha}\right]^{-1} \left[\boldsymbol{\chi} + \boldsymbol{c\xi}\right], \tag{7}$$

where $\mathbf{I}$ is the identity matrix, $\boldsymbol{\chi}$ is the differential irreversible susceptibility, and $\boldsymbol{\xi}$ is the differential anhysteretic susceptibility:

$$\boldsymbol{\chi} = \begin{cases} \boldsymbol{\chi_f} \dfrac{\boldsymbol{\chi}_f}{\|\boldsymbol{\chi}_f\|} & \text{if } (\boldsymbol{M_{an}} - \boldsymbol{M}) \partial \boldsymbol{H_{eff}} > 0, \\ 0 & \text{otherwise,} \end{cases}$$

$$\boldsymbol{\chi_f} = \boldsymbol{k}^{-1}\left(\boldsymbol{M_{an}} - \boldsymbol{M}\right), \; \boldsymbol{\xi} = \frac{\partial \boldsymbol{M}_{\rm an}}{\partial \boldsymbol{H}_{\rm eff}}, \; \boldsymbol{H}_{\rm eff} = \boldsymbol{H} + \boldsymbol{\alpha M}$$

where $\boldsymbol{\chi}_{\rm f}$ is an auxiliary vector quantity, $\boldsymbol{M}_{\rm an}$ is the anhysteretic magnetization, and $\boldsymbol{H}_{\rm eff}$ is the effective magnetic field strength. The model parameters $\boldsymbol{k}$, $\boldsymbol{\alpha}$, and $\boldsymbol{c}$ describe respectively, the pinning of domain walls, the Weiss domain co-operation, and the bulging of domain walls [7], [27].

For an isotropic magnetic material, the parameters of the JA model are scalars. However, experience has shown that a single set of parameters produces inaccurate results if used to fit all the symmetric minor BH loops [28]. Thus, in this paper, the parameters of the JA model are estimated for each measured symmetric minor BH loops. In the anisotropic case, the parameters are assumed to be symmetric tensors with entries

$$\boldsymbol{k} = \begin{bmatrix} k_x & 0 \\ 0 & k_y \end{bmatrix}, \; \boldsymbol{\alpha} = \begin{bmatrix} \alpha_x & 0 \\ 0 & \alpha_y \end{bmatrix}, \; \boldsymbol{c} = \begin{bmatrix} c_x & 0 \\ 0 & c_y \end{bmatrix}.$$

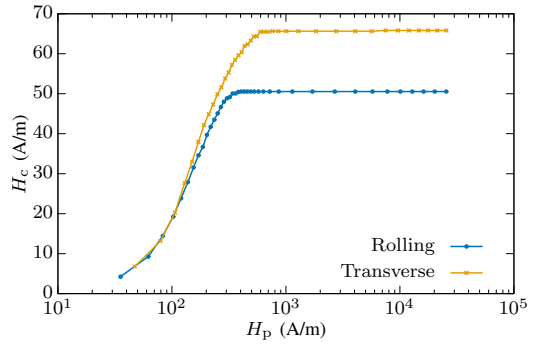

Fig. 3. The measured coercive field strength H_c represented as a function of the peak amplitude of magnetic field strength H_p.

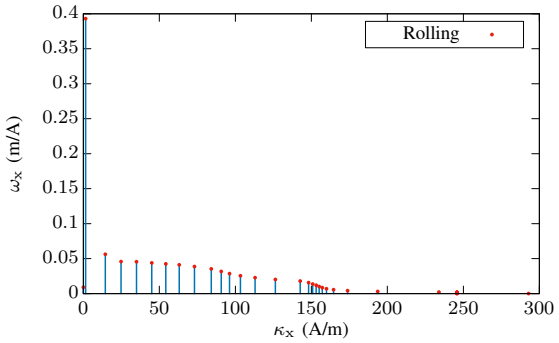

Fig. 4. The identified pinning field probability density for rolling direction. The total number of units (or cells) N = 44.

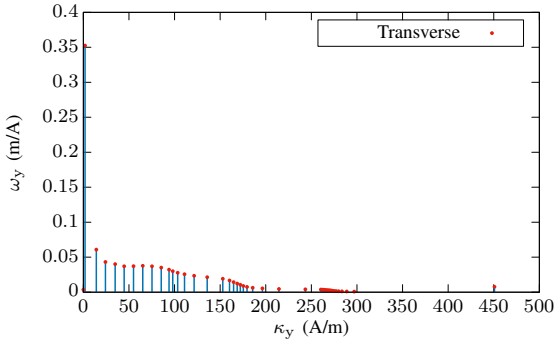

Fig. 5. The identified pinning field probability density for transverse direction. The total number of units (or cells) N = 44.

IV. Anhysteretic Characteristic

The classical Langevin and Brillouin functions are commonly used to represent the anhysteretic magnetic characteristics [7], [28]. However, these functions, or their combinations, cannot always fit with the measurements [29]. In this paper, the average curve of a measured major BH loop is assumed to be a close approximation of the anhysteretic magnetic behavior. The average curve is identified from unidirectional alternating magnetic measurements in the rolling and transverse directions. Computationally, the anhysteretic curve is represented by a shape-preserving cubic spline (see Fig. 2) [30]. In addition, the anhysteretic curve is linearly extrapolated in the region outside the measurement range.

Note that the JA model recognizes the interaction between neighbouring domains, so an inter-domain coupling field $\boldsymbol{\alpha M}$ is added to the applied magnetic field strength (see Section III) [7]. Although the formulations presented in preceding section (see Section II) neglect any interaction between domains, it is essential to apply the inter-domain coupling field for a better description of the magnetic characteristics. Adding the coupling field in the EB model leads to an implicit condition, and the condition in the update rule (4) evaluates to $\|[\boldsymbol{\kappa}^\ell]^{-1}(\boldsymbol{H}+\boldsymbol{\alpha M}-\boldsymbol{H}^\ell_{\mathrm{rev},t})\| \leq 1$, so (1) must be solved iteratively.

We first assume $\boldsymbol{\alpha}=0$ for the EB model and identify the inter-domain coupling parameter for the JA model. Then, the identified $\boldsymbol{\alpha}$ from the JA model is applied to the EB model, and the magnetic flux density is sought as a fixed point of the recursive relationship

$$\boldsymbol{B}^{l+1}_{t+\Delta t} = g(\boldsymbol{B}^{l}_{t+\Delta t}), \tag{8}$$

where $l=0,1,\ldots,l_{\max}$ is the iteration index, and g is the mapping function. The initial guess $\boldsymbol{B}^0_{t+\Delta t}$ is obtained from the solution of the explicit EB model (i.e., $\alpha=0$).

V. Parameter Identification

A. The EB Model Parameters

The parameters of the EB model are identified using the auxiliary function approach described in [12]. For the ℓ^{th} sub-region, the pinning field strength and its corresponding probability density is obtained by utilizing the following equations:

$$\omega^\ell = \int_{H^{\ell-1}}^{H^\ell} \omega(\kappa)\,\mathrm{d}\kappa = \frac{\partial F(H^\ell)}{\partial H} - \frac{\partial F(H^{\ell-1})}{\partial H}, \tag{9}$$

$$\kappa^\ell = \frac{\int_{H^{\ell-1}}^{H^\ell}\omega(\kappa)\kappa\,\mathrm{d}\kappa}{\int_{H^{\ell-1}}^{H^\ell}\omega(\kappa)\,\mathrm{d}\kappa} = \left[H\frac{\partial F(H)}{\partial H} - F(H)\right]_{H^{\ell-1}}^{H^\ell}, \tag{10}$$

where $F(H)$ is the auxiliary function. It is identified utilizing the measured $H_c(H_p)$ characteristic (see Fig. 3):

$$F(H_p^\ell) = \begin{cases} \dfrac{1}{2}F(H_p^{\ell-1}), & \text{if } H_p^\ell = \dfrac{1}{2}\left[H_p^{\ell-1} + H_c(H_p^{\ell-1})\right], \\ H_p^\ell - H_{c,\max}, & \text{if } H_p^\ell > H_{p,\max}. \end{cases} \tag{11}$$

The value of the characteristic function $H_c(H_p)=0$ at the origin, and for the section $(0, H_{p,\min}]$, it is assumed to behave quadratically,

$$H_c = H_{c,\min}\left(\frac{H_p}{H_{p,\min}}\right)^2,\ \forall H_p < H_{p,\min}.$$

The identified parameters of the EB model are shown in Fig. 4 and 5. It can be seen that some of the values of ω_x and ω_y become very small (almost negligible) if the number of cells are increased from 44. Therefore, the total number of cells $N=44$ is accepted as an optimal value.

Typically, the magnetic field strength is the most uncertain part of BH loop measurements [16]. Obviously, the coercive field is very small compared to the peak field strength and

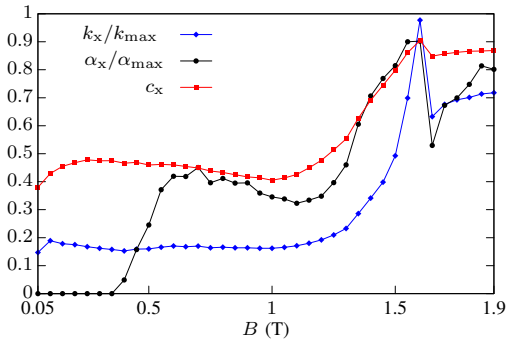

Fig. 6. Identified parameters of the JA model for rolling direction [Note: The normalization factor $k_{\max} = 540$ A/m and $\alpha_{\max} = 45 \times 10^{-6}$].

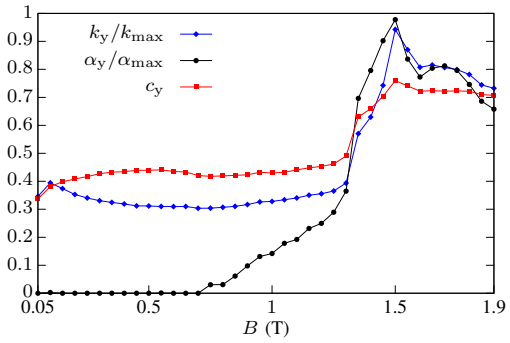

Fig. 7. Identified parameters of the JA model for transverse direction [Note: The normalization factor $k_{\max} = 350$ A/m and $\alpha_{\max} = 45 \times 10^{-6}$].

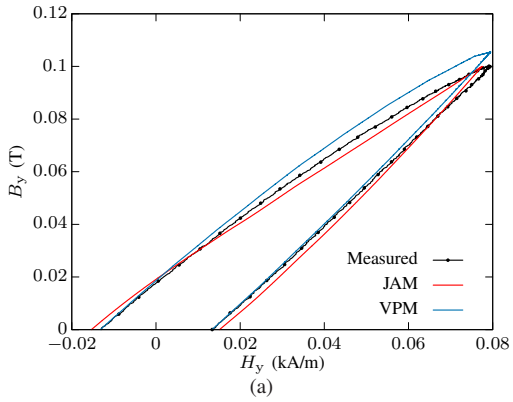

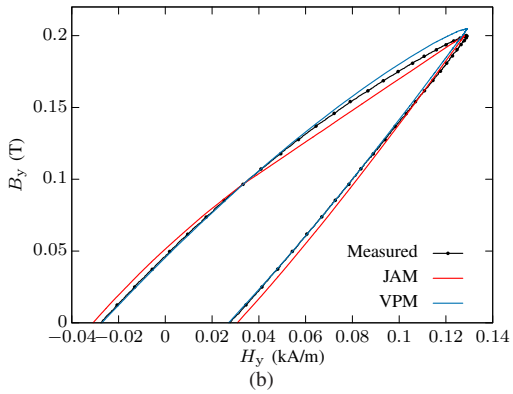

Fig. 8. Simulated and measured BH loops for low field excitations (transverse direction). (a) $B_{\text{peak}} = 0.1$ T. (b) $B_{\text{peak}} = 0.2$ T.

thus more prone to measurement uncertainty. Although it is difficult to quantify the exact measurement uncertainty, the differences between the rolling and transverse directions can be clearly distinguished (see Fig. 2 and 3).

B. The JA Model Parameters

Fig. 6 and 7 show the identified parameters of the JA model. Unlike in the classical approach, k_x, k_y, α_x, α_y and c_x, c_y are estimated for each of the measured symmetric minor BH loops. The larger number of parameters produce a better fit with the measured data. It is worth noting that the "loop-dependent" parameters are actually more physical than having a single set of parameters identified from only one major BH loop [28]. The variation in the parameters of the JA model improves both the reversible and irreversible susceptibility. As a result, the model produces a better fit with the measured symmetric minor loops (see Section VI).

The parameters of the JA model are estimated using a combination of global and local optimization techniques. The Simulated Annealing (SA) optimization method is used to obtain the initial estimate [14]. The results obtained from the SA method are refined using the Nelder-Mead-simplex (NMS) method [15], [30]. The mean square error is used as the cost function for the SA and NMS optimization algorithms.

The parameters k_x, k_y and c_x, c_y are related to the coercive field strength. Thus, changes in coercive field strength (see Fig. 3) reflect the changes in the pinning parameter [7]. Since the field strength $\boldsymbol{\alpha M}$ is a consequence of the averaged interaction between the domain magnetization, it is usually assumed to remain constant [7], [27]. However, the applied field reorients the domain magnetic moments through domain wall motion and moment rotation; therefore, the number of magnetic domains vary in accordance with the direction and amplitude of the applied field [32]. Hence, changes in domain wall configurations could affect the interactions between the domain magnetization. Therefore, the changes in the interactions between the domain magnetizations can be accounted for by allowing $\boldsymbol{\alpha}$ to vary with the applied input excitation (see Fig. 6 and 7) [31].

VI. Results and Discussion

A comparison between the simulation and measured unidirectional alternating BH loci is shown in Fig. 8 and 9. Given the number of identified parameters for EB and JA models, the simulation results are in good agreement with the unidirectional alternating measurements. However, the loss loci show some disagreements for high amplitude symmetric minor loops. The disagreement is better visualized in the hysteresis losses (see Fig. 10). It is worth noting that the simulation results from the JA model show much better agreement with the measured data. The reason behind is that the parameters for each measured symmetric minor loop are optimized separately.

On the other hand, the EB model reproduces a close approximation to the measured losses for the BH loops with the peak amplitude of flux density up to 1.4 T. At a higher amplitude of the input excitation, the error between the simulated and

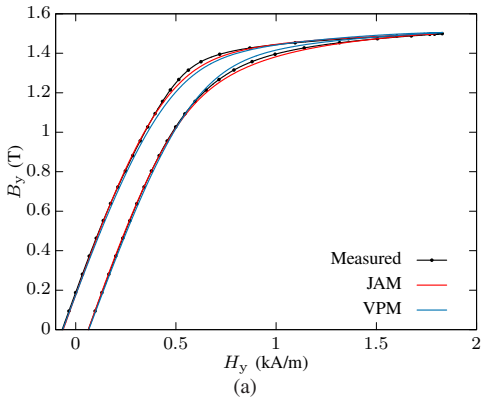

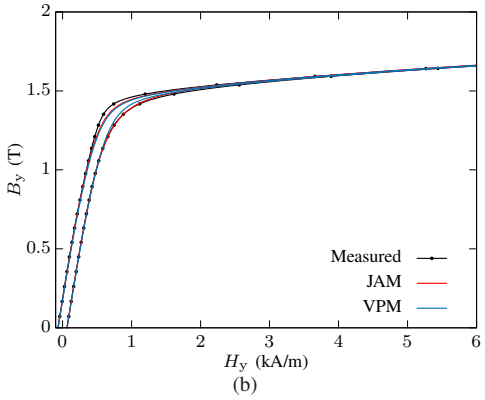

Fig. 9. BH-loops for high field excitations (transverse direction). (a) $B_{\text{peak}} = 1.5$ T. (b) $B_{\text{peak}} = 1.9\,\text{T},\ H_{\text{peak}} = 17.73$ kA [Note: The peak value of H is quite large, so some parts of the measured and simulated data are clipped for visualization.]

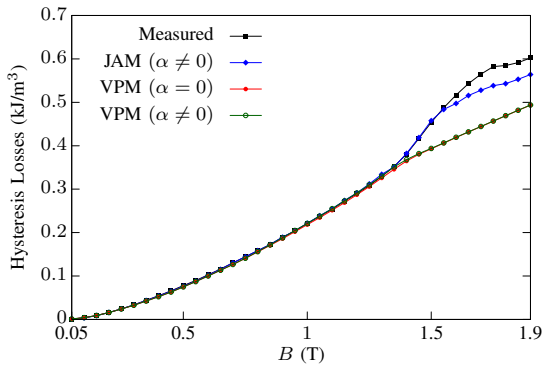

Fig. 10. Hysteresis losses for alternating field excitations (transverse direction).

measured BH loop is higher for the EB model, compared to the JA model. It is worth to note that the comparison is based on the fixed number of units (cells, $N = 44$). Therefore, two more tests are performed with new sets of EB model parameters. The first set consists of 62 cells and the second 83. However, the improvement is negligible, compared to the results with 44 cells. In contrast, small improvement is seen in the results with $\alpha \neq 0$, compared to $\alpha = 0$ (see Fig. 10).

The results for the rotational input excitations are shown in Fig. 11 and 12, and the losses in Fig. 13. It is interesting to note that the simulation results from the anisotropic two-axis model follows the measured loss loci until 1 T and increases

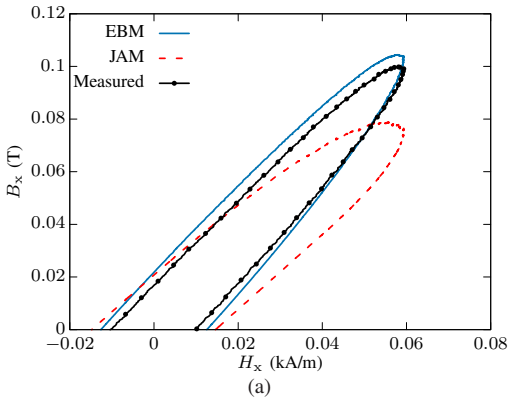

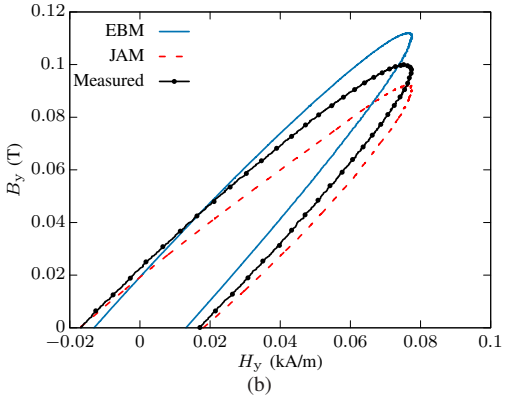

Fig. 11. Results for rotational low field excitation $|\boldsymbol{B}| = 0.1$ T. (a) $H_{\text{x}}B_{\text{x}}$-loci (b) $H_{\text{y}}B_{\text{y}}$-loci.

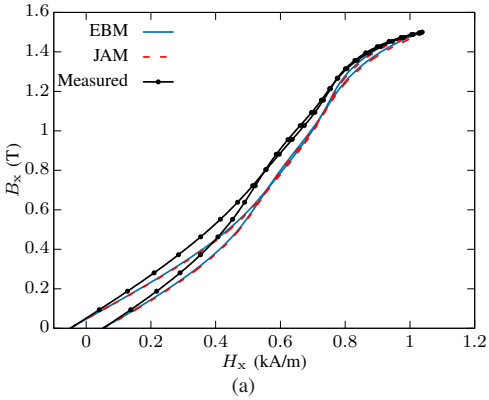

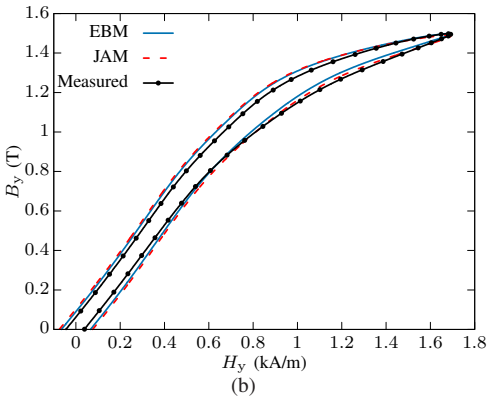

Fig. 12. Results for rotational high field excitation $|\boldsymbol{B}| = 1.5$ T. (a) $H_{\text{x}}B_{\text{x}}$-loci (b) $H_{\text{y}}B_{\text{y}}$-loci.

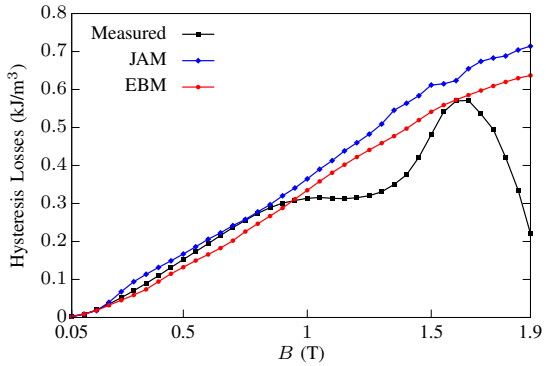

Fig. 13. Hysteresis losses for rotational field excitations. The simulated results are obtained from anisotropic EB and JA models.

linearly for higher input excitations. The anisotropic extension based on the magnetic characteristics from the rolling and transverse directions can produce either (i) circular output loci for circular input excitations (identical rolling and transverse characteristics), and (ii) elliptical output loci for circular input excitations or vice-versa (transverse characteristics are different from the rolling). Unlike in the unidirectional case, the measured rotational loss loci show non-monotonic behavior (see Fig. 13).

At high field excitations, fewer but larger domains occur, leading to a smaller number of domain walls. Hence the dissipative losses, which are a consequence of irreversible domain wall translation and rotation decreases. In contrast, the number of domains varies considerably under unidirectional alternating field excitation. Therefore, loss loci are monotonically increasing (see Fig. 10). Nevertheless, the microstructure and crystallographic texture affect the magnetic characteristics [32]. The simulation results confirm that the two-axis EB and JA models are suitable for modeling rotational losses only up to 1 T (see Fig. 13). Thus, it is required to have more information (parameters from other directions) for modeling losses occurring at higher rotational input excitations.

The modeling of rotational field variations and the losses are still challenging. The past studies suggest that both the EB (isotropic and with multi-cell approach) and JA models are unable to correctly represent the rotational field variations, specifically the decreasing trend in rotational losses at high field excitations [4], [26]. In contrast, the VPM with play hysterons shows acceptable results for both alternating and rotational field variations [33]. Likewise, the vector extension of the Preisach model (widely known as the Mayergoyz vector model [5]) shows proper fitting even for decreasing rotational loss loci at saturation [17], [34]. However, unlike the physical EB and JA models, the Mayergoyz vector model must be fine-tuned from a large set of measurement data.

VII. Conclusion

Simulation results from both the EB and JA models are compared with the measurement data. The BH loci and the hysteresis losses are compared for both unidirectional and rotational input excitations. Also, the hysteresis models are further extended to account for the magnetic anisotropy. The simulations show that both the models produce close approximations to the measured unidirectional alternating fields; however, at high field excitations, some discrepancies are visible. On the other hand, based on the rolling and transverse direction parameters, results from the simplified anisotropic extension lack adequate fit to the rotational $H_{\mathrm{x}}B_{\mathrm{x}}$, $H_{\mathrm{y}}B_{\mathrm{y}}$ loci and losses. Nevertheless, based on the simulated results, we can conclude that the two-axis (rolling-transverse) anisotropic EB and JA models are applicable when the rotational flux density is less than 1 T.

Acknowledgment

This work is supported by the Foundation for Aalto University Science and Technology. We would like to acknowledge the computational resources provided by the Aalto Science-IT project.

References

[1] A. Bergqvist, "Magnetic vector hysteresis model with dry friction-like pinning," *Physica B: Condensed Matter*, vol. 233, no. 4, pp. 342-347, 1997.
[2] A. Bergqvist, A. Lundgren, and G. Engdahl, "Experimental testing of an anisotropic vector hysteresis model," *IEEE Trans. on Magn.*, vol. 33, no. 5, pp. 4152-4154, 1997.
[3] F. Henrotte, A. Nicolet, and K. Hameyer, "An energy-based vector hysteresis model for ferromagnetic materials," *COMPEL-Int. J. Comput. Math. Elect. Electron. Eng.*, vol. 25, no. 1, pp. 71-80, 2006.
[4] F. Henrotte and K. Hameyer, "A dynamical vector hysteresis model based on an energy approach," *IEEE Trans. Magn.*, vol. 42, no. 4, pp. 899-902, 2006.
[5] I. D. Mayergoyz, "Mathematical Models of Hysteresis," New York, NY, USA: Springer, 1991.
[6] A. Sutor, J. Kallwies, and R. Lerch, "An efficient vector Preisach hysteresis model based on novel rotational operator," *J. Appl. Phys.*, vol. 111, no. 7, pp. 07D106, 2012.
[7] D. C. Jiles and D. L. Atherton, "Ferromagnetic hysteresis," *IEEE Trans. Magn.*, vol. 19, no. 5, pp. 2183-2185, 1983.
[8] K. Jacques, R. Sabariego, C. Geuzaine, and J. Gyselinck, "Inclusion of a direct and inverse energy-consistent hysteresis model in dual magnetostatic finite element formulations," *IEEE Trans. Magn.*, vol. 52, no. 3, pp. 7300304, 2016.
[9] E. Dlala, J. Saitz, and A. Arkkio, "Inverted and forward Preisach models for numerical analysis of electromagnetic field problems," *IEEE Trans. Magn.*, vol. 42, no. 8, pp. 1963-1973, 2006.
[10] S. Bi, A. Sutor, R. Lerch, and Y. Xiao, "An efficient inverted hysteresis model with modified switch operator and differentiable weight function," *IEEE Trans. Magn.*, vol. 49, no. 7, pp. 3175-3178, 2013.
[11] J. V. Leite, N. Sadowski, P. Kuo-Peng, N. J. Batistela, and J. P. A. Bastos, "Inverse Jiles-Atherton vector hysteresis model," *IEEE Trans. Magn.*, vol. 40, no. 4, pp. 1769-1775, 2004.
[12] K. Jacques, S. Steentjes, F. Henrotte, C. Geuzaine, and K. Hameyer, "Representation of microstructural features and magnetic anisotropy of electrical steels in an energy-based vector hysteresis model," *AIP Advances*, vol. 8, no. 5, pp. 047602, 2018.
[13] D. Lederer, H. Igarashi, A. Kost, and T. Honma, "On the parameter identification and application of the Jiles-Atherton hysteresis model for numerical modeling of measured characteristics," *IEEE Trans. Magn.*, vol. 35, no. 3, pp. 1211-1214, 1999.
[14] C. R. Reeves, "Modern heuristic techniques for combinatorial problems," *McGraw-Hill*, 1995.
[15] J. A. Nelder and R. Mead, "A simplex method for function minimization," *Computer Journal*, vol. 7, no. 4, pp. 308-313, 1965.
[16] V. Goričan, A. Hamler, B. Hribernik, M. Jesenik, and M. Trlep, "2-D measurements of magnetic properties using a round RSST," *Proc. 6th Intl. Workshop 1 & 2-Dimensional Magn. Meas. Test.*, Bad Gastein, Austria, 2000, pp. 66-75.
[17] P. Handgruber, A. Stermecki, O. Bíró, V. Goričan, E. Dlala, and G. Ofner, "Anisotropic generalization of vector Preisach hysteresis models for nonoriented steels," *IEEE Trans. Magn.*, vol. 51, no. 3, p. 1-4, 2015.

[18] F. Fiorillo and A. Novikov, "An improved approach to power losses in magnetic laminations under nonsinusoidal induction waveform," *IEEE Trans. Magn.*, vol. 26, no. 5, pp. 2904-2910, 1990.
[19] L. Prigozhin, V. Sokolovsky, J. W. Barrett, and S. E. Zirka, "On the energy-based variational model for vector magnetic hysteresis," *IEEE Trans. Magn.*, vol. 52, no. 12, pp. 7301211, 2016.
[20] S. Steentjes, F. Henrotte, C. Geuzaine, and K. Hameyer, "A dynamical energy-based hysteresis model for iron loss calculation in laminated cores," *Int. J. Numer. Model.*, vol. 27, no. 3, pp. 433-443, 2013.
[21] K. Jacques, "Energy-Based Magnetic Hysteresis Models - Theoretical Development and Finite Element Formulations," Ph.D. dissertation, Université de Liège, Liège, Belgique, 2018 [Online]. Available: http://hdl.handle.net/2268/229596
[22] R. P. Brent, "An algorithm with guaranteed convergence for finding a zero of a function," *Computer Journal*, vol. 14, no. 4, pp. 422-425, 1971.
[23] D. Lin and P. Zhou, "A practical anisotropic vector hysteresis model based on play hysterons," *IEEE Trans. Magn.*, vol. 53, no. 1, pp. 7301206, 2017.
[24] D. Lin, P. Zhou, and A. Bergqvist, "Improved vector play model and parameter identification for magnetic hysteresis materials," *IEEE Trans. Magn.*, vol. 50, no. 2, pp. 7008704, 2014.
[25] S. Steentjes, F. Henrotte, and K. Hameyer, "Energy-based ferromagnetic material model with magnetic anisotropy," *J. Magn. Magn. Mater.*, vol. 425, pp. 20-24, 2017.
[26] A. Bergqvist, "A simple vector generalization of the Jiles-Atherton model of hysteresis," *IEEE Trans. Magn.*, vol. 32, no. 5, pp. 4213-4215, 1996.
[27] C. S. Schneider, S. D. Gedney, S. M. Joyce, T. W. Fulton, and M. A. Travers, "Measurement and exponential model of ferromagnetic hysteresis," *Physica B: Condensed Matter*, vol. 570, pp. 259-265, 2019.
[28] Z. Gmyrek, "Numerical modeling of static hysteresis loop using variable parameters," *Int. J. Numer. Model.*, vol. 27, no. 2, pp 199-212, 2013.
[29] S. Steentjes, M. Petrun, G. Glehn, D. Dolinar, and K. Hameyer, "Suitability of the double Langevin function for description of anhysteretic magnetization curves in NO and GO electrical steel grades," *AIP Advances*, vol. 7, no. 5, pp. 056013, 2017.
[30] M. Galassi *et al.*, *GNU Scientific Library Reference Manual* (3rd Ed.), ISBN 0954612078. [Online]. Available: http://www.gnu.org/software/gsl/
[31] B. Kavasnica and F. Kundracík, "Fitting experimental anhysteretic curves of ferromagnetic materials and investigation of the effect of temperature and tensile stress," *J. Magn. Magn. Mater.*, vol. 162, no. 1, pp. 43-49, 1996.
[32] A. Hubert and R. Schäfer, "Magnetic Domains: The Analysis of Magnetic Microstructures," Springer Science & Business Media, 2008.
[33] T. Matsuo and M. Miyamoto, "Dynamic and anisotropic vector hysteresis model based on isotropic vector play model for nonoriented silicon steel sheet," *IEEE Trans. Magn.*, vol. 48, no. 2, pp. 215-218, 2012.
[34] E. Dlala, "Magnetodynamic Vector Hysteresis Models for Steel Laminations of Rotating Electrical Machines," Ph.D. dissertation, Helsinki University of Technology, Espoo, Finland, 2008 [Online]. Available: https://aaltodoc.aalto.fi/handle/123456789/3011